A Dual-Fluorescence Assay for Gene Delivery Vehicle Screening in Macrophages with an Inflammation-Inducible Reporter Construct

Allie Ivy[1], Shelby N Bess[1], Shilpi Agrawal[1], Varun Kochar[2], Timothy J Muldoon[1], Christopher E. Nelson[*1]

[1]University of Arkansas, Biomedical Engineering
[2]Joint Department of Biomedical Engineering, University of North Carolina at Chapel Hill and North Carolina State University, Chapel Hill, 27599, NC, United States

***Address for correspondence**
Christopher E. Nelson, Ph.D.
Department of Biomedical Engineering
120 John A. White Jr. Engineering Hall
University of Arkansas
Fayetteville, AR 72701
479-575-2615
nelsonc@uark.edu

Abstract

Macrophages are a promising target for therapeutics in various applications such as regenerative medicine and immunotherapy for cancer. Due to their plastic nature, macrophages can switch from a non-activated state to activated with the smallest environmental change. For macrophages to be effective in their respective applications, screening for phenotypic changes is necessary to elucidate the cell response to different delivery vehicles, vaccines, small molecules, and other stimuli. We created a sensitive and dynamic high-throughput screening method for macrophages based on the activation of NF-κB. For this reporter, we placed an mCherry fluorescence gene under the control of an inflammatory promoter, which recruits NF-κB response elements to promote expression during the inflammatory response in macrophages. We characterized the inflammatory reporter based on key markers of an inflammatory response in macrophages including TNF-α cytokine release and immunostaining for inflammatory and non-inflammatory cell surface markers. With the inflammatory reporter, we also were able to create an LPS dose curve to determine the dynamic range of the reporter and determine the sensitivity of the reporter to stimulus through timepoint analysis of stimulus vs. non-stimulus treated reporter cells. We then used the reporter cell line to determine both delivery efficiency and inflammatory response to different viral and non-viral gene delivery vehicles. Thie screening technique developed here provides a dynamic, high-throughput screening technique for determining inflammatory response by mouse macrophages to specific stimuli and provides insight into the inflammatory response of mouse macrophages to different viral and non-viral gene delivery methods.

Introduction

Macrophages are phagocytic cells responsible for defense against foreign invaders and maintaining homeostasis in all organs and tissues[1–3]. Based on the microenvironment, macrophages change function to respond to local need. The plasticity of macrophages leads to a heterogenous population of macrophage phenotypes to address the situation, whether defense, maintenance, or in transition between activation states. Macrophages play a role in tumors as tumor-associated macrophages (TAMS) and regenerative processes in the body. For many cancers, macrophages are abundant in the tumor microenvironment and TAMS are responsible for facilitating metastasis, immunosuppression, and promoting invasion and angiogenesis[4]. Macrophages are also responsible for maintaining the healing process from initial inflammation to remove foreign invaders, recruiting necessary immune cells, and resolving the healing process in the end stages of regeneration[5–9].

Macrophages can participate in a wide variety of activities due to their ability to switch between activation states. Understanding of macrophage polarization state is continually evolving and at the most basic level is either a classically activated/inflammatory or alternatively activated/anti-inflammatory state. These states have also been described as M0 (resting), M1 (inflammatory), and M2 (anti-inflammatory). Due to their utility, macrophages have been targeted for use in many different applications from cell therapy for oncology to reprogramming the local environment in regeneration[10–16]. Although macrophages provide a

range of utility, their ability to switch between an activated and alternatively activated state provides challenges in adapting these cells for use in different therapeutic applications. With the advent of genetically engineered macrophage cell therapy[16], the role of delivering gene-editing machinery to macrophages has been of increasing interest as viral and non-viral delivery methods can prove to be highly inflammatory.

The landscape of different gene-editing tools available for use has dramatically changed over the past few decades. These new tools and techniques provide a way to both investigate and manipulate cellular behavior and are invaluable in the development of therapeutics targeting and using macrophages. So far, macrophage gene expression has been manipulated using shRNA[17], siRNA[18–20], zinc-fingers (ZFNs)[21], transcriptional activator-like effector nucleases (TALENs)[22,23], and CRISPR-Cas9[24–26]. And yet, delivery of gene-editing tools remains a challenge. Due to the innate nature of macrophages to respond to foreign invaders, many viral and non-viral delivery vehicles lead to an inflammatory response[16,27]. Although this may be desirable for some approaches, as mentioned before, many therapeutic applications that would benefit from macrophage manipulation require an anti-inflammatory phenotype favoring regenerative processes, such as for chronic wounds[9], skeletal muscle damage following injury[28], myocardial infarction[29–31], impaired liver regeneration[32], and even brain damage[33,34].

For cancer immunotherapy, inflammatory macrophages are beneficial as that is the desired state for the cell therapeutic, but for regenerative approaches, an inflammatory macrophage phenotype would prove detrimental to the continued healing process. It is essential to determine the effects of different delivery modalities on macrophages before attempting to manipulate them with current gene-editing technology.

To screen the inflammatory response of macrophages to different delivery vehicles, we developed a high-throughput screening method that relays the inflammatory response of RAW264.7 mouse macrophage cells to viral and non-viral delivery methods. Others have taken similar approaches to investigate macrophage inflammatory responses using nuclear factor kappa B (NF-κB) reporters, an important transcription factor for the inflammatory response, to determine which genes regulate inflammatory pathways in macrophages[35]. Here, we establish a high-throughput screening technique to determine macrophage inflammatory response via the NF-κB activation pathway. We then used the high-throughput screen for viral and non-viral delivery vehicles to determine their effect on macrophage activation.

Results

Inflammatory Reporter Characterization

To achieve high-throughput screening of macrophage's inflammatory response to external elements, an inflammatory reporter plasmid was constructed. The coding sequence for mCherry fluorescent protein placed under an inflammation-inducible promoter from Jadav and Truong[36] using Gibson cloning. The inflammatory promoter contained 14 NF-κB transcription factors with a minimal CMV promoter. The plasmid also contained lentivirus packaging elements with puromycin resistance under an Ef1α promoter to maintain expression over time (**Fig. 1A**). The plasmid sequence was validated using Sanger sequencing. To evaluate the inflammatory reporter, it was stably integrated in RAW264.7s, a mouse macrophage cell line, using lentiviral transduction[37]. Following puromycin selection, the RAW264.7-Inflammatory reporter cells (RAW264.7-IRCs) were stimulated using lipopolysaccharide (LPS) from *E. coli and* sorted for the top 10% of mCherry expressing cells to ensure a more homogenous population.

Dynamic Range of Inflammatory Reporter

We assessed the dynamic range of the reporter in response to increasing levels of stimuli. The RAW264.7- IRCs were stimulated using LPS. RAW264.7-IRCs were seeded in 24-well plates. Dose levels ranged from 0.001 ng/mL to 100 ng/mL of LPS (**Fig. 1B**). 24 hours post-treatment, reporter cells were harvested in PBS, as described previously, and mCherry expression levels were quantified using flow cytometry. Cells were discarded after analysis. The data collected was analyzed using FlowJo™ v10.8 Software (BD Life Sciences). Cells were gated first to determine live cells by forward (FSC-A) and side scatter (SSC-A) and then FSC-A and FSC-H for single cells. Cells were then evaluated for mCherry

expression (SSC v. mCherry). Geometric mean values reported in the dose curve were taken from the single cell data. A dose response curve showing the dynamic range of the inflammatory reporter based on the geometric mean of the mCherry fluorescence seen in the single cell data set showed a dynamic response range from 0.1-1 ng/mL for the RAW264.7-IRCs (**Fig. 1B**). We also used ELISA to determine TNF-α levels in response to LPS activation for dose levels 0.001-1 ng/mL. Media from the RAW264.7-IRC cells used for the dose curve was collected before the cells were harvested and used to determine TNF-α levels released by the macrophages following 24 hours of LPS stimulation. TNF-α levels increased significantly over the dynamic range 0.1-1.0 ng/mL LPS, which aligns with the increasing inflammatory response seen by the inflammatory reporter across that range of LPS stimulation (**Fig. 1B&C**). To show the comparison between mCherry fluorescent geometric mean and TNF-α cytokine release by the RAW264.7-IRCs, the two values were plotted against each other and showed a linear correlation between the two values, with an R-squared value of 0.90 (**Fig. 1D**).

Responsiveness of Inflammatory Reporter

The responsiveness of the inflammatory reporter was tested under LPS and interferon gamma (IFN-γ) stimulus. On day 0, RAW264.7-IRCs were treated with LPS and IFN-γ. 24-hours post-treatment, the 24h timepoint cells were harvested for flow cytometry, as described previously, and mCherry expression was quantified using the gating strategy described above. At this time, the media containing the stimuli for the 48h and 72h timepoint cells were removed and replaced with fresh media. 48h and 72h timepoint cells were harvested and mCherry expression quantified via flow cytometry (**Fig. 1E**). The inflammatory reporter showed a significant increase between the geometric mean intensity of the non-treated cells versus the treated cells (LPS, IFN-γ) 24 hours post-stimulus, as expected. At 48- and 72-hours post-treatment and the removal of the stimulus, there was a decrease in mCherry expression so that there was little to no significant difference seen between non-treated and previously treated RAW264.7-IRCs, showing that the reporter is responsive to the changing activation states of the macrophage (**Fig. 1F**).

Phenotyping RAW264.7-IRCs using Immunostaining

Immunostaining was performed to characterize the phenotypic surface expression 24 hours post-cytokine stimulation of the RAW264.7-IRCs. RAW264.7-IRC cells were treated with LPS at a concentration of 10 ng/mL for 24 hours prior to fixing and staining the cells with CD86 and CD206 to determine whether the cell populations exhibited a more inflammatory (M1) or anti-inflammatory (M2) phenotype based on cell surface markers CD86 is a common marker of classically activated mouse macrophages and CD206 is a common marker for alternatively activated mouse macrophages[38]. RAW264.7-IRCs stimulated with LPS showed a mixed phenotype displaying both the CD86 and CD206, like untreated RAW264.7-IRCs (**Fig. 2A**). Co-localization analysis of mean fluorescent intensity of mCherry with CD86 (blue) and CD206 (green) was performed using Fiji[39]. Co-localization analysis was performed for both non-stimulated RAW264.7-IRCs (**Fig. 2B**) and LPS-stimulated RAW264.7-IRCs (**Fig. 2C)**. For non-stimulated, mCherry fluorescence was minimized and there is more co-expression of both CD206 and CD86. For LPS-stimulated cells, there was an increase in CD86 mean fluorescent intensity, while CD206 decreased in mean fluorescent intensity. LPS stimulated cells exhibited an inflammatory phenotype, but mCherry expression is not as high as expected for this population although there is a trend towards increased mCherry expression. As the ratio of the fluorescent intensities of CD86:CD206 (a ratio of M1:M2) increased, mCherry fluorescence increased, but there was also a population with an increased inflammatory phenotype that do not have an increased mCherry fluorescence (**Fig. 2D**).

Inflammatory response of RAW264.7-IRCs to various viral and non-viral delivery methods

Viral and non-viral delivery vehicles were screened using RAW264.7-IRCs to determine the level of immune activation in response to the vehicles. For viral delivery, adeno-associated virus (AAV) serotypes 1, 2, 5, 8, and 9 at an MOI of 38,000, where MOI was determined based on the mass ratio of AAV to adenovirus, and adenovirus serotype 5/35 (Ad5/35) at an MOI of 1,000 were used to transduce the inflammatory reporter cells with a CMV promoter-driven green fluorescent protein (GFP). For non-viral delivery, Lipofectamine™ 2000 and TransIT-X2® Dynamic Delivery System (Mirus bio), a polymer with proprietary components that aid in cell uptake, were used to deliver a plasmid encoding CMV promoter-

driven GFP to RAW264.7-IRCs. Cells receiving viral delivery were analyzed using flow cytometry to quantify GFP and mCherry levels at both 24- and 48 hours post-transduction. Cells were harvested for flow cytometry and mCherry and GFP fluorescence was quantified. Cells transfected with non-viral delivery vehicles were harvested and GFP and mCherry fluorescence analyzed via flow cytometry at 48-hours post-transfection, per the respective manufacturer's protocol. Using both GFP and mCherry, the dual-reporter assay elucidated both delivery efficiency based on GFP levels and inflammatory response based on mCherry levels. Following flow cytometry, data was analyzed using FlowJo™ Software with the same gating process mentioned above with an additional step of gating on a quadrant of GFP vs. mCherry. **Figure 3A** shows the percentage of cells in each quadrant (q1: mCherry-/GFP-; q2: mCherry+/GFP-; q3: mCherry+/GFP+; q4: mCherry-/GFP+). There was no observable difference between AAV2, AAV5, AAV8, AAV9, and the control in inflammatory response. AAV2, AAV5, AAV8, and AAV9 also showed no GFP delivery to the RAW264.7- IRCs. AAV1 showed a slight increase in GFP delivery with an average of 25.9% GFP+ cells. As expected, Ad5/35 showed a significant increase in the efficiency of GFP delivery with an average of 56.4% GFP+ cells, but interestingly, the delivery vehicle was only slightly more inflammatory than others with an average 75.4% mCherry+ cells compared to 61.2% for reporter control. Similarly, to what was seen in **Figure 1E**, AAV2, AAV5, AAV8, and AAV9 showed a relative decrease in mCherry+ cells, illustrating a return to an alternatively activated state. Ad5/35 had the most significant GFP expression with an average of 56.4% and 45.1% GFP+ cells at 24h and 48h, respectively, and increased mCherry expression compared to reporter control at 24h (75.4% vs. 61.2%). Interestingly, the reporter control maintained its inflammatory response compared to treatment groups which averaged a 22.5% decrease in %mCherry+ from 24h to 48h. TransIT-X2 delivery of GFP resulted in efficient GFP delivery (35.8% GFP+), but also significantly increased inflammatory response (95.2% mCherry+) versus reporter control at 48h (67.9% mCherry+). Lipofectamine 2000 delivery resulted in an inflammatory response like TransIT-X2 delivery, with 96.2% mCherry+ and less efficient GFP delivery with 20.5% GFP+.

Delivery data was plotted to show the ratio of efficient delivery to inflammatory response using the fluorescence geometric mean values for both GFP and mCherry (GFP Geometric Mean:mCherry Geometric Mean) (**Fig. 3B**). Geometric means were used to represent the data due to the wide range of fluorescent intensities in the sample cells and to lessen the effects of extreme outliers in the flow data, namely with the non-viral delivery, such as with TransIT-X2 (**Fig. 3C**). Again, Ad5/35 presents the only viable option for both efficient delivery and a lower inflammatory response, whereas with non-viral delivery, Lipofectamine 2000 and TransIT-X2, there is a higher delivery efficiency but also significantly increased inflammatory response to these modes of delivery. Interestingly, when graphing the geometric means, the reporter control shifts drastically from the 24h to the 48h data set and shows an increased GFP geometric mean of 198.8 vs. 380.8, respectively, and increased mCherry geometric mean of 380.8 vs. 690.4, indicating a heightened inflammatory state. This phenomenon was further studied by looking at the effects of confluency on mCherry expression and inflammatory state of the RAW264.7-IRCs (**Fig. S1**). To determine the effects of confluency on the baseline mCherry fluorescence, RAW264.7-IRCs were seeded in 12-well plates to achieve 10% to 90% confluency. Those cells were then harvested at 24h and 48h post-seeding for flow sorting. The results showed a general upward trend in both %mCherry+ cells and mCherry fluorescent geometric mean. Overall, depending on the time points and confluency, the range for %mCherry positive was around 20% to 40% and geometric mean ranged from 200 to almost 400 across both time points and different confluencies (**Fig. S1**).

Discussion

As therapeutics continue to advance, it is important to continually develop tools that aid in their rapid development. Macrophages represent a compelling target for regenerative and immunomodulatory therapeutics due to their innate nature as they both defend the body and facilitate the return to and maintenance of homeostasis[9]. It is essential to know how macrophages will respond to different therapeutics including small molecule drugs, gene delivery vehicles, or new vaccines. In the early development stage, high-throughput screening techniques, such as the one described here, could provide simultaneous results on gene delivery and inflammatory responses for candidate vectors.

The reporter developed here can be used to investigate the role of inflammation through the NF-κB activation pathway, which is important in regulating the expression of various inflammatory genes, including TNF-α[40–42]. The RAW264.7-IRCs utilize the NF-κB activation pathway through the 14 NF-κB response elements to promote mCherry expression. This in turn relays the relative amount of inflammation due to activated NF-κB, that has translocated to the nucleus. We were able to confirm the inflammatory status of the RAW264.7-IRCs and their relative mCherry expression to TNF-α released by the cells at different LPS doses (**Fig. 1B&C**). The inflammatory reporter is both responsive and titratable. The LPS dose curve and TNF-α concentration curve corresponding to the same LPS doses, ranging from 0.001 to 1 ng/mL, show that the mCherry expression is strongly correlated with the common inflammatory marker, TNF-α. The reporter shows a responsiveness to its environment and can recover from inflammatory stimulus back to baseline levels, which is in line with the plastic nature of macrophages (**Fig. 1E**). Interestingly, through immunostaining for macrophages markers CD86 (M1) and CD206 (M2), we saw similar phenotypes with both markers expressed on both non-treated and LPS treated RAW264.7-IRCs, which could be due to the nature of the RAW264.7 cell line to exist as phenotypically diverse at baseline. RAW264.7 cells are an immortalized cell line and experience a more homogenous NF-κB response than primary macrophages. RAW264.7 cells exhibit a lower basal activated (nuclear) NF-κB level at about 5-10% of total cellular NF-κB compared to bone-marrow derived mouse macrophages (BMMs) with a higher basal activated NF-κB level at 25-35% of total cellular NF-κB. Also of note, RAW264.7s only reached 50-60% of total cellular NF-κB translocation to the nucleus upon LPS stimulation whereas BMMs achieved activated NF-κB levels of 80-90% of total cellular NF-κB[43]. The basal levels of activated NF-κB could also contribute to the levels of mCherry expression observed in non-treated RAW264.7-IRCs, especially in those seeded for an optimal confluency.

In order to draw meaningful conclusions, a non-stimulated RAW264.7-IRC control should be used for every experiment to normalize the inflammation experienced by the cells due to environmental factors such as confluency, which was determined to be a contributor to mCherry expression and can result in a range of basal mCherry expression of 20-40% mCherry+ cells or a geometric mean for mCherry fluorescence ranging from 250-400 (**Fig. S1**). These macrophages represent a very heterogenous population and tend to change size and morphology upon stimulation. Due to this, the geometric mean was used to account for extremes in the different populations and compare the bulk of the phenotypes seen in each treatment group during flow cytometry analysis. The geometric mean weights the mean fluorescent intensity based on the bulk cell population and gives less weight to the upper extremity of the distribution. This was especially important when comparing treatments such as TransIT-X2 and Lipofectamine 2000 to the other groups as a small portion of RAW264.7-IRCs expressed much higher levels of mCherry (**Fig. 3C**).

After characterizing the inflammatory reporter cell line, the RAW264.7-IRCs were used for a dual-reporter assay to determine inflammatory response in macrophages to different viral and non-viral delivery vehicles and delivery efficiency. The various delivery vehicles had an array of effects on activation of the mouse macrophages, ranging from some viral vectors showing zero effect on the macrophages, with basal mCherry levels and no GFP expression, to the non-viral vectors showing both increased delivery and greatly increased inflammation. Using the RAW264.7-IRCs to investigate the effects of various delivery vectors, both viral and non-viral, we saw that AAV serotypes 1,2, 5, 8, and 9 had no effect on either delivery or inflammatory response by the macrophages. AAV1 showed an increase in both GFP and mCherry fluorescence compared to the other AAV serotypes tested. In comparing the transduction efficiency of AAV1 across timepoints and the drastic change in the control RAW264.7-IRCs from 24 to 48 hours, it is difficult to draw conclusions on the effectiveness of that specific vector. As expected, Ad5/35 had the best GFP delivery for the macrophages due to the engineering of the adenovirus to target CD46, which is expressed by macrophages, and increasing the level of uptake in those cells[16,44]. Ad5/35 is used in the production of chimeric antigen receptor macrophages (CAR-Ms) which are macrophages that are modified *ex vivo* before being transduced back into the patient to target cancers, and as such must maintain an inflammatory (M1) macrophage phenotype to induce an immune response in the tumor microenvironment. The issue with the viral vectors that lead to more efficient delivery is the inflammatory response associated with their use. For some applications, such as with CAR-Ms for immunotherapy in cancer, an inflammatory phenotype is desirable due to the immunosuppressive nature of tumors and a need to mount a response to the tumor[45–47]. Although this may be the goal for some therapeutics, other

approaches may require an anti-inflammatory phenotype for the macrophages post-delivery with viral or non-viral vehicles. This approach is especially important for a regenerative medicine setting where inflammation, both acute and chronic, is usually the cause for prolonged healing processes or pathologic fibrosis[3,48,49]. Either way, the reporter developed here can provide insight into inflammatory or anti-inflammatory nature of delivery vehicles and aide in high-throughput screening for rapid candidate development.

In summary, this inflammatory reporter provides a sensitive and dynamic screening tool to determine the response to different stimuli and reveal information on inflammatory responses by macrophages. As for future studies, this inflammatory reporter can be used in different applications when looking at inflammatory response or processes related to NF-κB activation. One study used an NF-κB reporter for CRISPR knockout screening to determine different genes important to inflammatory response and essential for viability in macrophages[35]. This reporter could also provide insights for small molecules screening on inflammation[50] or elucidate the effects of vaccines on macrophages during development[51,52]. Overall, this work demonstrates a well-characterized screening technique for inflammatory response in macrophages that can be useful in gene delivery and adoptive cell therapy.

Methods

Cell lines

The RAW264.7 murine macrophage cell line was purchased from the American Type Culture Collection (ATCC TIB-71). These cells were cultured in Dulbecco's modified Eagle's medium (DMEM) (Gibco) with 10% fetal bovine serum (FBS) (Gibco) and 1% penicillin/streptomycin (P/S) (Gibco). Cells were grown in a tissue culture incubator at 37°C and 5% CO2. Cells were passaged using a cell scraping method to resuspend the adherent cells.

Plasmid construction

The inflammatory reporter plasmid was constructed with mCherry red fluorescent protein under a previously described synthesis-friendly inflammation-inducible promoter (SFNp) with puromycin resistance under a PGK promoter and lentivirus packaging elements. The plasmid pLenti-CMV-GFP-Puro (Addgene #17448) containing lenti packaging elements, GFP under a CMV promoter and puromycin resistance under a PGK promoter, was used as the backbone. The CMV-GFP was removed from the plasmid using ClaI and SalI and purified via gel electrophoresis. The mCherry red fluorescent protein was taken from the pU6-pegRNA-GG-acceptor plasmid (Addgene #132777) via PCR using Q5 High-Fidelity DNA Polymerase (NEB) and purified. The SFNp sequence was ordered as a gene block from Integrated DNA Technologies (IDT). The SFNp sequence is:

```
GGATCCACGGGATACCCCAGGGGCTCTCCAGGGAATCTCCGGGGATACTCCAGGGGGTTTCCGGGGAATCC
CCCGGGAGTTTCCTGGGAATTTCCCGGGATTTCCCCGGGGCATCCCGGGGACTCTCCTGGGATTTTCCAGG
GACATTCCTGGGACTTTCCTGCGCGGTAGGCGTGTACGGTGGGAGGTCTATATAAGCAGAGCTCGTTTAGT
GAACCGTCAGATCGCCTGGAGACGCCATCCACGCTGTTTTGACCTCCATAGAAGACACCGGGACCGATCCA
GCCTCTCGACATTCGTGCCACCATG
```
[36].

Overhangs were added to the gene block via PCR and purified. All PCR primers for overhangs were designed using NEBuilder Assembly Tool. NEB Gibson Assembly® Master Mix was used to combine the fragments according to manufacturer's instructions.

Stable cell culture creation using lentivirus

The inflammatory reporter plasmid was used to create a stably expressing cell line via lentiviral infection, using the 2nd generation lentiviral system including psPAX2 (Addgene #12260), pMD2.G (Addgene #12259), and the inflammatory reporter plasmid. HEK293T cells were seeded in 10cm plates at a seeding density of 2 million cells. At 75-90% confluency, all three plasmids were transfected into HEK293 cells using calcium phosphate precipitation transfection. Media was changed 16 hours post-transfection, and media containing lentivirus was harvested at 24- and 48-hours post-media change. Supernatant containing lentivirus was then filtered using a 0.45 µm cellulose acetate filter. Lenti-X concentrator was added to the filtered viral supernatant at a 1:4 ratio and stored at 4°C overnight. The following morning, the centrifuge was cooled to 4°C and the virus was centrifuged at 1,500x*g* for 45 minutes. Supernatant was aspirated and pellet resuspended in PBS at 20x the volume of the original viral media. RAW264.7 cells were seeded in 5cm plates at a seeding density of 800,000 cells. At 75% confluency, lentivirus containing the inflammatory reporter was added. Viral media was replaced with fresh media 24-hours post-transduction. The cells were allowed to expand for another 24- to 48-hours before puromycin selection occurred with a concentration of 3.5 µg/ml for one week. Following puromycin selection, cells were activated using LPS at 1 ng/ml over 24-hours before using flow sorting to obtain the top 10% of mCherry expressing cells. Cells were expanded and then cryo-preserved for future use.

Viral Transduction of RAW264.7-IRCs

RAW264.7-IRCs were seeded in 24-well plates at a seeding density of 50,000 cells per well. At 75% confluency, media was changed 2-hours before transfection. The RAW264.7-IRCs were transduced with AAV 1, 2, 5, 8, and 9, all containing a GFP construct (UNC Vector Core), and Adenovirus 5/35 (Ad5/35)-GFP (Welgen, Inc.). Inflammatory reporter RAW264.7 cells were transduced at an MOI of 38,000 for all AAV serotypes and 1,000 for Ad5/35[16]. Transfection media was replaced with fresh media 24 hours post-treatment and cells were allowed to expand for another 24- or 48- hours, respectively, before harvesting cells for flow cytometry.

Non-Viral Transfection of RAW264.7-IRCs

RAW264.7-IRCs were seeded in 24-well plates at a seeding density of 50,000 cells per well. At 75% confluency, media was changed 2-hours before transfection. Transfection using Lipofectamine™ 2000 (ThermoFisher) and TransIT-X2® Dynamic Delivery System (Mirus bio), were carried out per manufacturer instructions. Briefly, 5 µg of an expression plasmid containing GFP was diluted in Opti-MEM™ Reduced Serum Medium (Gibco™) and mixed with Lipofectamine 2000 diluted in Opti-MEM. The DNA/Lipofectamine 2000 mixture was incubated for 5 minutes at room temperature before being added to the RAW264.7-IRCs. Cells were incubated for 48 hours before harvesting. For TransIT-X2, it was brought to room temperature and vortexed prior to use. 1.5 µg of pDNA was diluted in 150uL Opti-MEM. 4.5 µl of TransIT-X2 was then added to the diluted DNA mixture and incubated for 15-30 minutes at room temperature before being split evenly across three wells. Cells were incubated for 48 hours before harvesting.

Flow cytometry

All flow cytometry experiments were performed using the MA900 instrument (Sony Biotechnology). All cells were re-suspended in Dulbecco's phosphate buffered saline (PBS) (ThermoFisher) via scraping methods prior to sorting. Samples were strained using EASYstrainer Cell Sieves 40 µm (Greiner Bio-One). All stimulated RAW264.7-IRCs were evaluated alongside unstimulated RAW264.7-IRCs and RAW264.7 cells lacking any reporter for initial gating and to set the mCherry- gate. Cells were gated first to determine live cells by forward (FSC-A) and side scatter (SSC-A) and then FSC-A and FSC-H for single cells. Cells were then evaluated for mCherry (SSC v. mCherry) and/or GFP expression (SSC v. GFP). Cells were discarded after flow cytometry analysis. Further information on the gating strategy can be found in **Supplementary Figure S2**. All data was evaluated using FlowJo™ Software.

Immunostaining

Immunostaining was performed to characterize phenotypic surface expression post-cytokine stimulation. AlexaFluor™ 647 secondary antibody with CD86 primary antibody was used to detect CD86, a common M1 marker, and AlexaFluor™ 488 secondary antibody with CD206 primary antibody was used to detect CD206, a common M2 marker. The RAW264.7-IRCs were seeded in 35 mm glass bottom MatTek dishes, P35G-1.5-10-C (MatTek Life Sciences) at a seeding density of 300,000 cells per dish, 24 hours prior to cytokine stimulation. 24-hours post-cytokine stimulation, cells were fixed in 10% neutral buffered formalin and permeabilized using 0.2% Triton-X 100, followed by blocking with 2% bovine serum albumin (BSA) for 60 minutes. The primary antibodies were added and allowed to incubate overnight at 4°C. Cells were then washed with phosphate buffered saline (PBS) prior to imaging. Images were acquired using an inverted laser scanning confocal microscope (Olympus Fluoview FV10i-LiV) with a 60X (1.2□N.A., water immersion).

TNF-α ELISA

RAW264.7-IRCs were seeded in 24-well plates at a seeding density of 50,000 cells/well. 24-hours after seeding, cells were washed with PBS and media was replaced with stimulating media at varying doses of LPS (0.001 ng/mL to 1 ng/mL) for 24-hours. Supernatant was collected and spun down to remove any cellular debris and then frozen at -80°C prior to use. The cell culture supernatant was thawed and diluted 1:10. TNF-α levels were measured using the TNF alpha Mouse Elisa Kit (Invitrogen) according to manufacturer instructions. Fluorescent readouts were analyzed using a BioTek Synergy LX multi-mode reader (Agilent), measured at 450nm. The standard curve was graphed and used to determine the concentration of TNFα of each sample. Concentrations were corrected for dilution factor.

Acknowledgement

Conflict of interest

There are no conflicts to report.

Author contributions

AI and CN designed experiments and wrote the manuscript. AI performed experiments, analyzed data, and created figures. SB performed immunostaining and confocal imaging. TJM assisted with confocal analysis, experimental design for macrophage imaging, and manuscript revisions. VK aided in confocal imaging.

REFERENCES

1. Chen, S., Yang, J., Wei, Y., and Wei, X. (2020). Epigenetic regulation of macrophages: from homeostasis maintenance to host defense. Cell. Mol. Immunol. *17*, 36–49. https://doi.org/10.1038/s41423-019-0315-0.

2. Verschoor, C.P., Puchta, A., and Bowdish, D.M.E. (2012). The Macrophage. In Leucocytes: Methods and Protocols Methods in Molecular Biology., R. B. Ashman, ed. (Humana Press), pp. 139–156. https://doi.org/10.1007/978-1-61779-527-5_10.

3. Murray, P.J., and Wynn, T.A. (2011). Protective and pathogenic functions of macrophage subsets. Nat. Rev. Immunol. *11*, 723–737. https://doi.org/10.1038/nri3073.

4. Noy, R., and Pollard, J.W. (2014). Tumor-associated macrophages: from mechanisms to therapy. Immunity *41*, 49–61. https://doi.org/10.1016/j.immuni.2014.06.010.

5. Leibovich, S.J., and Ross, R. (1975). The role of the macrophage in wound repair. A study with hydrocortisone and antimacrophage serum. Am. J. Pathol. *78*, 71–100.

6. Subramaniam, M., Saffaripour, S., Van De Water, L., Frenette, P.S., Mayadas, T.N., Hynes, R.O., and Wagner, D.D. (1997). Role of endothelial selectins in wound repair. Am. J. Pathol. *150*, 1701–1709.

7. Nagaoka, T., Kaburagi, Y., Hamaguchi, Y., Hasegawa, M., Takehara, K., Steeber, D.A., Tedder, T.F., and Sato, S. (2000). Delayed Wound Healing in the Absence of Intercellular Adhesion Molecule-1 or L-Selectin Expression. Am. J. Pathol. *157*, 237–247.

8. Mori, R., Kondo, T., Ohshima, T., Ishida, Y., and Mukaida, N. (2002). Accelerated wound healing in tumor necrosis factor receptor p55-deficient mice with reduced leukocyte infiltration. FASEB J. Off. Publ. Fed. Am. Soc. Exp. Biol. *16*, 963–974. https://doi.org/10.1096/fj.01-0776com.

9. Krzyszczyk, P., Schloss, R., Palmer, A., and Berthiaume, F. (2018). The Role of Macrophages in Acute and Chronic Wound Healing and Interventions to Promote Pro-wound Healing Phenotypes. Front. Physiol. *9*, 419. https://doi.org/10.3389/fphys.2018.00419.

10. Fidler, I.J. (1974). Inhibition of pulmonary metastasis by intravenous injection of specifically activated macrophages. Cancer Res. *34*, 1074–1078.

11. Jetten, N., Roumans, N., Gijbels, M.J., Romano, A., Post, M.J., de Winther, M.P.J., van der Hulst, R.R.W.J., and Xanthoulea, S. (2014). Wound Administration of M2-Polarized Macrophages Does Not Improve Murine Cutaneous Healing Responses. PLoS ONE *9*, e102994. https://doi.org/10.1371/journal.pone.0102994.

12. Ruffell, B., Affara, N.I., and Coussens, L.M. (2012). Differential Macrophage Programming in the Tumor Microenvironment. Trends Immunol. *33*, 119–126. https://doi.org/10.1016/j.it.2011.12.001.

13. Squadrito, M.L., and De Palma, M. (2011). Macrophage regulation of tumor angiogenesis: implications for cancer therapy. Mol. Aspects Med. *32*, 123–145. https://doi.org/10.1016/j.mam.2011.04.005.

441 14. Mosser, D.M., and Edwards, J.P. (2008). Exploring the full spectrum of macrophage activation. Nat.
442 Rev. Immunol. *8*, 958–969. https://doi.org/10.1038/nri2448.

443 15. Lee, S., Kivimäe, S., Dolor, A., and Szoka, F.C. (2016). Macrophage-Based Cell Therapies: The Long
444 and Winding Road. J. Control. Release Off. J. Control. Release Soc. *240*, 527–540.
445 https://doi.org/10.1016/j.jconrel.2016.07.018.

446 16. Klichinsky, M., Ruella, M., Shestova, O., Lu, X.M., Best, A., Zeeman, M., Schmierer, M., Gabrusiewicz,
447 K., Anderson, N.R., Petty, N.E., et al. (2020). Human chimeric antigen receptor macrophages for
448 cancer immunotherapy. Nat. Biotechnol. *38*, 947–953. https://doi.org/10.1038/s41587-020-0462-y.

449 17. Surdziel, E., Clay, I., Nigsch, F., Thiemeyer, A., Allard, C., Hoffman, G., Reece-Hoyes, J.S., Phadke, T.,
450 Gambert, R., Keller, C.G., et al. (2017). Multidimensional pooled shRNA screens in human THP-1 cells
451 identify candidate modulators of macrophage polarization. PLOS ONE *12*, e0183679.
452 https://doi.org/10.1371/journal.pone.0183679.

453 18. Kaushal, D., Gupta, S., and Pathak, Y.V. (2022). Delivery of siRNA to Macrophages: Challenges and
454 Opportunities. In Macrophage Targeted Delivery Systems: Basic Concepts and Therapeutic
455 Applications, S. Gupta and Y. V. Pathak, eds. (Springer International Publishing), pp. 469–487.
456 https://doi.org/10.1007/978-3-030-84164-5_21.

457 19. Domschke, G., Linden, F., Pawig, L., Hafner, A., Akhavanpoor, M., Reymann, J., Doesch, A.O., Erbel, C.,
458 Weber, C., Katus, H.A., et al. (2018). Systematic RNA-interference in primary human monocyte-
459 derived macrophages: A high-throughput platform to study foam cell formation. Sci. Rep. *8*, 10516.
460 https://doi.org/10.1038/s41598-018-28790-3.

461 20. Lai, Y., Xu, X., Zhu, Z., and Hua, Z. (2018). Highly efficient siRNA transfection in macrophages using
462 apoptotic body-mimic Ca-PS lipopolyplex. Int. J. Nanomedicine *13*, 6603–6623.
463 https://doi.org/10.2147/IJN.S176991.

464 21. Liang, J., Wang, J., Azfer, A., Song, W., Tromp, G., Kolattukudy, P.E., and Fu, M. (2008). A Novel CCCH-
465 Zinc Finger Protein Family Regulates Proinflammatory Activation of Macrophages *. J. Biol. Chem.
466 *283*, 6337–6346. https://doi.org/10.1074/jbc.M707861200.

467 22. Kuhn, A., Ackermann, M., Mussolino, C., Cathomen, T., Lachmann, N., and Moritz, T. (2017). TALEN-
468 mediated functional correction of human iPSC-derived macrophages in context of hereditary
469 pulmonary alveolar proteinosis. Sci. Rep. *7*, 15195. https://doi.org/10.1038/s41598-017-14566-8.

470 23. Chen, M., Zhu, H., Mao, Y., Cao, N., Yu, Y., Li, L., Zhao, Q., Wu, M., and Ye, M. (2020). Regulation of
471 IL12B Expression in Human Macrophages by TALEN-mediated Epigenome Editing. Curr. Med. Sci. *40*,
472 900–909. https://doi.org/10.1007/s11596-020-2249-2.

473 24. Navarro-Guerrero, E., Tay, C., Whalley, J.P., Cowley, S.A., Davies, B., Knight, J.C., and Ebner, D. (2021).
474 Genome-wide CRISPR/Cas9-knockout in human induced Pluripotent Stem Cell (iPSC)-derived
475 macrophages. Sci. Rep. *11*, 4245. https://doi.org/10.1038/s41598-021-82137-z.

476 25. Dong, Y., Zhang, S., Gao, X., Yin, D., Wang, T., Li, Z., Wan, Z., Wei, M., Luo, Y., Yang, G., et al. (2021).
477 HIF1α epigenetically repressed macrophages via CRISPR/Cas9-EZH2 system for enhanced cancer
478 immunotherapy. Bioact. Mater. *6*, 2870–2880. https://doi.org/10.1016/j.bioactmat.2021.02.008.

26. Lee, Y.-W., Mout, R., Luther, D.C., Liu, Y., Castellanos-García, L., Burnside, A.S., Ray, M., Tonga, G.Y., Hardie, J., Nagaraj, H., et al. (2019). In Vivo Editing of Macrophages through Systemic Delivery of CRISPR-Cas9-Ribonucleoprotein-Nanoparticle Nanoassemblies. Adv. Ther. *2*, 1900041. https://doi.org/10.1002/adtp.201900041.

27. Chuang, S.T., Stein, J.B., Nevins, S., Kilic Bektas, C., Choi, H.K., Ko, W.-K., Jang, H., Ha, J., and Lee, K.-B. Enhancing CAR Macrophage Efferocytosis Via Surface Engineered Lipid Nanoparticles Targeting LXR Signaling. Adv. Mater. *n/a*, 2308377. https://doi.org/10.1002/adma.202308377.

28. Arnold, L., Henry, A., Poron, F., Baba-Amer, Y., van Rooijen, N., Plonquet, A., Gherardi, R.K., and Chazaud, B. (2007). Inflammatory monocytes recruited after skeletal muscle injury switch into antiinflammatory macrophages to support myogenesis. J. Exp. Med. *204*, 1057–1069. https://doi.org/10.1084/jem.20070075.

29. van Amerongen, M.J., Harmsen, M.C., van Rooijen, N., Petersen, A.H., and van Luyn, M.J.A. (2007). Macrophage Depletion Impairs Wound Healing and Increases Left Ventricular Remodeling after Myocardial Injury in Mice. Am. J. Pathol. *170*, 818–829. https://doi.org/10.2353/ajpath.2007.060547.

30. Dick, S.A., Macklin, J.A., Link to external site, this link will open in a new window, Nejat, S., Link to external site, this link will open in a new window, Momen, A., Clemente-Casares, X., Althagafi, M.G., Chen, J., Link to external site, this link will open in a new window, et al. (2019). Self-renewing resident cardiac macrophages limit adverse remodeling following myocardial infarction. Nat. Immunol. *20*, 29–39. http://dx.doi.org/10.1038/s41590-018-0272-2.

31. Hilgendorf, I., Gerhardt, L.M.S., Tan, T.C., Winter, C., Holderried, T.A.W., Chousterman, B.G., Iwamoto, Y., Liao, R., Zirlik, A., Scherer-Crosbie, M., et al. (2014). Ly-6Chigh Monocytes Depend on Nr4a1 to Balance Both Inflammatory and Reparative Phases in the Infarcted Myocardium. Circ. Res. *114*, 1611–1622. https://doi.org/10.1161/CIRCRESAHA.114.303204.

32. Liu, R., Scimeca, M., Sun, Q., Melino, G., Mauriello, A., Shao, C., Shi, Y., Piacentini, M., Tisone, G., and Agostini, M. (2023). Harnessing metabolism of hepatic macrophages to aid liver regeneration. Cell Death Dis. *14*, 1–10. https://doi.org/10.1038/s41419-023-06066-7.

33. Feng, X., Frias, E.S., Paladini, M.S., Chen, D., Boosalis, Z., Becker, M., Gupta, S., Liu, S., Gupta, N., and Rosi, S. (2021). Functional role of brain-engrafted macrophages against brain injuries. J. Neuroinflammation *18*, 232. https://doi.org/10.1186/s12974-021-02290-0.

34. Kim, E., Yang, J., Beltran, C.D., and Cho, S. (2014). Role of Spleen-Derived Monocytes/Macrophages in Acute Ischemic Brain Injury. J. Cereb. Blood Flow Metab. *34*, 1411–1419. https://doi.org/10.1038/jcbfm.2014.101.

35. Covarrubias, S., Cortez Vollmers, A., Capili, A., Boettcher, M., Shulkin, A., Correa, M.R., Halasz, H., Robinson, E.K., O'Briain, L., Vollmers, C., et al. (2020). High-Throughput CRISPR Screening Identifies Genes Involved in Macrophage Viability and Inflammatory Pathways. Cell Rep. *33*, 108541. https://doi.org/10.1016/j.celrep.2020.108541.

36. Jadav, A., and Truong, K. (2021). Creation of a synthesis-friendly inflammation-inducible promoter suitable for cell therapy. Integr. Biol. *13*, 230–236. https://doi.org/10.1093/intbio/zyab015.

518 37. Dull, T., Zufferey, R., Kelly, M., Mandel, R.J., Nguyen, M., Trono, D., and Naldini, L. (1998). A third-
519 generation lentivirus vector with a conditional packaging system. J. Virol. *72*, 8463–8471.
520 https://doi.org/10.1128/JVI.72.11.8463-8471.1998.

521 38. Taciak, B., Białasek, M., Braniewska, A., Sas, Z., Sawicka, P., Kiraga, Ł., Rygiel, T., and Król, M. (2018).
522 Evaluation of phenotypic and functional stability of RAW 264.7 cell line through serial passages. PLoS
523 ONE *13*, e0198943. https://doi.org/10.1371/journal.pone.0198943.

524 39. Schindelin, J., Arganda-Carreras, I., Frise, E., Kaynig, V., Longair, M., Pietzsch, T., Preibisch, S., Rueden,
525 C., Saalfeld, S., Schmid, B., et al. (2012). Fiji: an open-source platform for biological-image analysis.
526 Nat. Methods *9*, 676–682. https://doi.org/10.1038/nmeth.2019.

527 40. Mussbacher, M., Derler, M., Basílio, J., and Schmid, J.A. (2023). NF-κB in monocytes and
528 macrophages – an inflammatory master regulator in multitalented immune cells. Front. Immunol.
529 *14*. https://doi.org/10.3389/fimmu.2023.1134661.

530 41. Wang, N., Liang, H., and Zen, K. (2014). Molecular mechanisms that influence the macrophage m1-
531 m2 polarization balance. Front. Immunol. *5*, 614. https://doi.org/10.3389/fimmu.2014.00614.

532 42. Liu, T., Zhang, L., Joo, D., and Sun, S.-C. (2017). NF-κB signaling in inflammation. Signal Transduct.
533 Target. Ther. *2*, 1–9. https://doi.org/10.1038/sigtrans.2017.23.

534 43. Bagaev, A.V., Garaeva, A.Y., Lebedeva, E.S., Pichugin, A.V., Ataullakhanov, R.I., and Ataullakhanov, F.I.
535 (2019). Elevated pre-activation basal level of nuclear NF-κB in native macrophages accelerates LPS-
536 induced translocation of cytosolic NF-κB into the cell nucleus. Sci. Rep. *9*, 4563.
537 https://doi.org/10.1038/s41598-018-36052-5.

538 44. Nilsson, M., Ljungberg, J., Richter, J., Kiefer, T., Magnusson, M., Lieber, A., Widegren, B., Karlsson, S.,
539 and Fan, X. (2004). Development of an adenoviral vector system with adenovirus serotype 35
540 tropism; efficient transient gene transfer into primary malignant hematopoietic cells. J. Gene Med.
541 *6*, 631–641. https://doi.org/10.1002/jgm.543.

542 45. Mitchem, J.B., Brennan, D.J., Knolhoff, B.L., Belt, B.A., Zhu, Y., Sanford, D.E., Belaygorod, L.,
543 Carpenter, D., Collins, L., Piwnica-Worms, D., et al. (2013). Targeting tumor-infiltrating macrophages
544 decreases tumor-initiating cells, relieves immunosuppression and improves chemotherapeutic
545 responses. Cancer Res. *73*, 1128–1141. https://doi.org/10.1158/0008-5472.CAN-12-2731.

546 46. Yang, L., Li, A., Lei, Q., and Zhang, Y. (2019). Tumor-intrinsic signaling pathways: key roles in the
547 regulation of the immunosuppressive tumor microenvironment. J. Hematol. Oncol.J Hematol Oncol
548 *12*, 125. https://doi.org/10.1186/s13045-019-0804-8.

549 47. Li, L., Yu, R., Cai, T., Chen, Z., Lan, M., Zou, T., Wang, B., Wang, Q., Zhao, Y., and Cai, Y. (2020). Effects
550 of immune cells and cytokines on inflammation and immunosuppression in the tumor
551 microenvironment. Int. Immunopharmacol. *88*, 106939.
552 https://doi.org/10.1016/j.intimp.2020.106939.

553 48. Smigiel, K.S., and Parks, W.C. (2018). Macrophages, Wound Healing, and Fibrosis: Recent Insights.
554 Curr. Rheumatol. Rep. *20*, 17. https://doi.org/10.1007/s11926-018-0725-5.

555 49. Wynn, T.A., and Vannella, K.M. (2016). Macrophages in tissue repair, regeneration, and fibrosis.
556 Immunity *44*, 450–462. https://doi.org/10.1016/j.immuni.2016.02.015.

557 50. Koch, P.D., Miller, H.R., Yu, G., Tallarico, J.A., Sorger, P.K., Wang, Y., Feng, Y., Thomas, J.R., Ross, N.T.,
558 and Mitchison, T. (2018). A High Content Screen in Macrophages Identifies Small Molecule
559 Modulators of STING-IRF3 and NFkB Signaling. ACS Chem. Biol. *13*, 1066–1081.
560 https://doi.org/10.1021/acschembio.7b01060.

561 51. Choi, H.-G., Choi, S., Back, Y.W., Park, H.-S., Bae, H.S., Choi, C.H., and Kim, H.-J. (2016).
562 Mycobacterium tuberculosis Rv2882c Protein Induces Activation of Macrophages through TLR4 and
563 Exhibits Vaccine Potential. PLOS ONE *11*, e0164458. https://doi.org/10.1371/journal.pone.0164458.

564 52. Yang, S.-J., Chen, Y.-Y., Hsu, C.-H., Hsu, C.-W., Chang, C.-Y., Chang, J.-R., and Dou, H.-Y. (2020).
565 Activation of M1 Macrophages in Response to Recombinant TB Vaccines With Enhanced
566 Antimycobacterial Activity. Front. Immunol. *11*. https://doi.org/10.3389/fimmu.2020.01298.

567
568

FIGURES

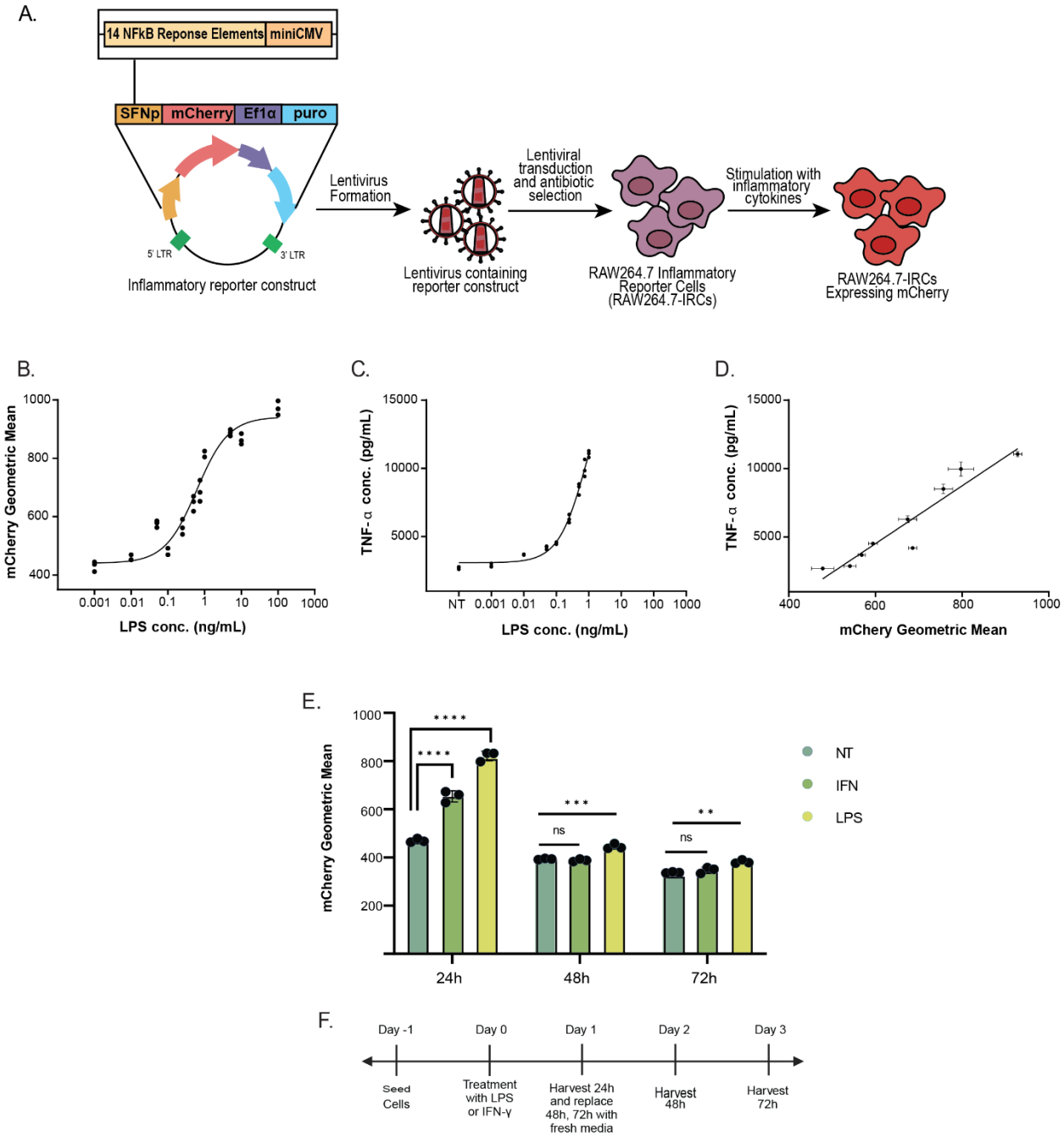

Figure 1. Characterization of RAW264.7-Inflammatory Reporter Cell line.
1A. Overview of RAW264.7-IRC cell line creation. The inflammatory reporter construct, created using Gibson cloning, contained an mCherry fluorescent reporter under an inflammatory promoter, termed synthesis friendly inflammatory promoter (SFNp)[36], and was encapsulated and transduced via lentivirus. The cells then underwent puromycin selection to create a homogenous population of cells. RAW264.7-IRCs were then stimulated using different cytokines and inflammatory agents to induce mCherry expression.
1B. LPS dose curve showing range of mCherry fluorescence geometric mean values measured using flow cytometry across a range of LPS doses from 0.001 to 100 ng/mL. Individual data points are plotted

for each biological replicate. Each dose was done in triplicate. Trend line calculated using the three-parameter dose-response curve, which yielded an EC50 = 0.61 ng/mL with an R^2 value of 0.94. Dose-response curve line equation can be found in **Table S1.**

1C. TNF-α concentration levels (pg/mL) in cell culture supernatant measured using ELISA. Cells were treated with LPS at concentrations ranging from 0.001 to 1 ng/mL for 24 hours. Each data point represents an average of 2 technical replicates. Trend line calculated using the three-parameter dose-response curve, which yielded an EC50 = 0.87 ng/mL with an R^2 value of 0.987. Dose-response curve line equation can be found in Table S2**.**

1D. Plot of mCherry fluorescent geometric mean values plotted against respective TNF-α concentration levels (pg/mL). *X*-values represent the average of the 3 biological replicates of TNF-α concentration (from Fig. 1C) and *y*-values represent the average of the 3 biological replicates of mCherry geometric mean (from Fig. 1B) ± SD. Trend line calculated using linear regression, $y = 21.12x-8156$, with an R^2 value of 0.90. Linear regression parameters can be found in Table S3.

1E. RAW264.7-IRC responsiveness. RAW264.7-IRCs were treated with LPS and IFN-γ for 24 hours, 24h cells were harvested for flow cytometry. Stimulation media was replaced with fresh media for the 48h and 72h samples. 24h post-removal of stimulation media, the 48h samples were harvested for flow cytometry, and the same was done for the 72h samples. Mean ± SD, with individual data points for each biological replicate. (**** p-value ≤ 0.0001, *** p-value ≤ 0.001, ** p-value ≤ 0.01, n.s. p-value > 0.05).

1F. Timeline of treatment for RAW264.7-IRC responsiveness.

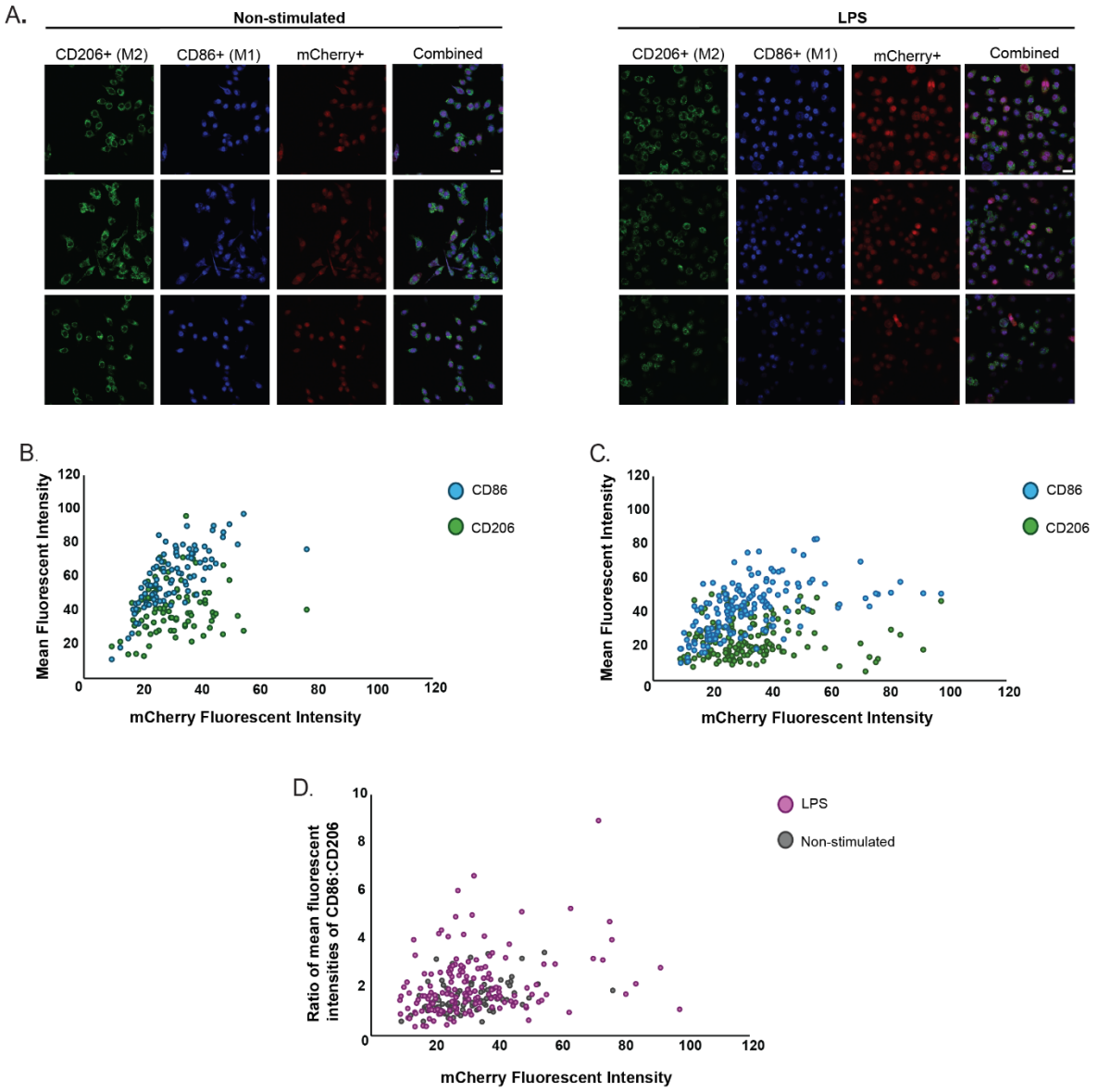

Figure 2. Immunostaining for Inflammatory versus Non-Inflammatory Phenotype in RAW264.7-IRCs

2A. Phenotyping via immunostaining of RAW264.7-IRCs for CD206 (green), a common anti-inflammatory marker, and CD86 (blue), a common inflammatory marker, co-localized with mCherry expression between no treatment and LPS treated cells (10ng/mL). Scale bars are 20 µm.

2B. Co-localization of CD86 and CD206 with mCherry expression in non-stimulated RAW264.7-IRCs.

2C. Co-localization of CD86 and CD206 with mCherry expression in LPS-stimulated RAW264.7-IRCs.

2D. Ratio of mean fluorescent intensities of CD86:CD206 to mCherry fluorescent intensity.

A.

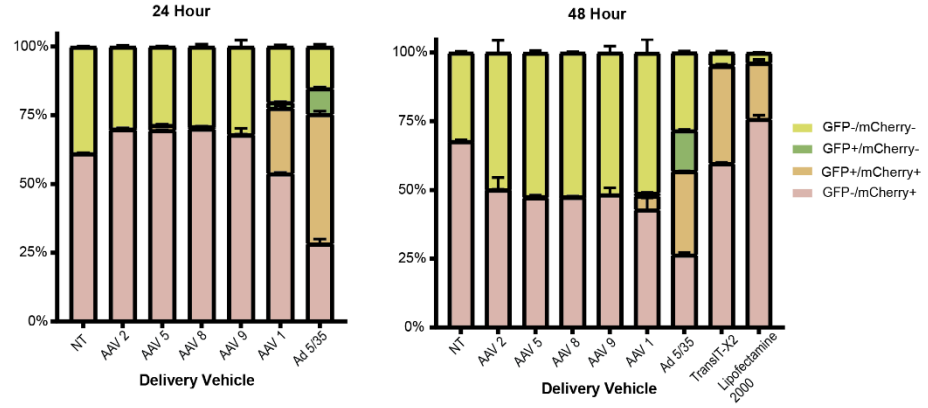
24 Hour
48 Hour
100%
75%
50%
25%
0%
NT
AAV 2
AAV 5
AAV 8
AAV 9
AAV 1
Ad 5/35
TransIT-X2
Lipofectamine 2000
Delivery Vehicle
GFP-/mCherry-
GFP+/mCherry-
GFP+/mCherry+
GFP-/mCherry+

B.

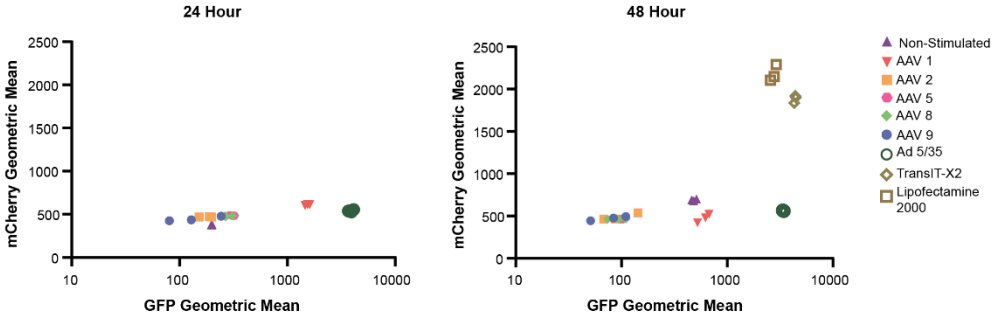
24 Hour
48 Hour
mCherry Geometric Mean
GFP Geometric Mean
2500
2000
1500
1000
500
0
10
100
1000
10000
Non-Stimulated
AAV 1
AAV 2
AAV 5
AAV 8
AAV 9
Ad 5/35
TransIT-X2
Lipofectamine 2000

C.

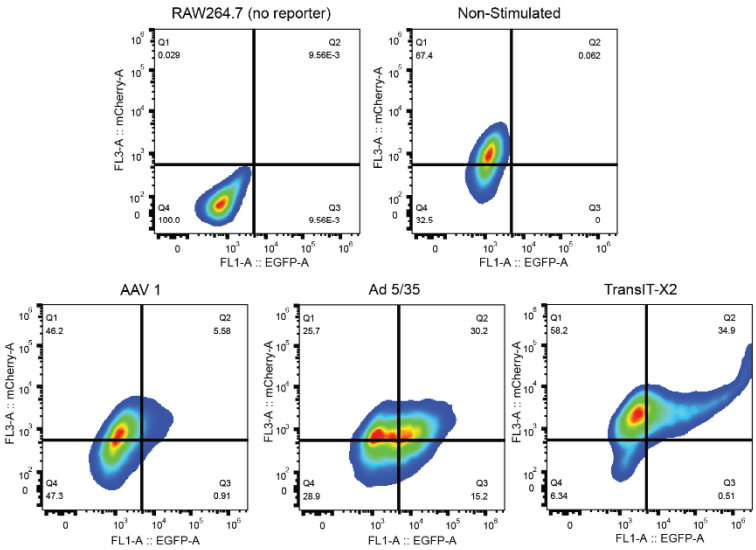
RAW264.7 (no reporter)
Non-Stimulated
AAV 1
Ad 5/35
TransIT-X2
FL3-A :: mCherry-A
FL1-A :: EGFP-A
Q1 0.029
Q2 9.56E-3
Q4 100.0
Q3 9.56E-3
Q1 67.4
Q2 0.062
Q4 32.5
Q3 0
Q1 46.2
Q2 5.58
Q4 47.3
Q3 0.91
Q1 25.7
Q2 30.2
Q4 28.9
Q3 15.2
Q1 58.2
Q2 34.9
Q4 6.34
Q3 0.51

617

Figure 3. Evaluation of Inflammatory Response and Delivery Efficiency of Viral and Non-Viral Delivery Vehicles using RAW264.7-IRCs

2A. Evaluation of viral and non-viral delivery methods using a dual-reporter assay at 24 and 48 hours post-delivery. Efficiency of delivery and inflammatory response were determined by using different viral (AAV 1, 2, 5, 8, 9 and Ad5/35) and non-viral (TransIT-X2 and Lipofectamine 2000) delivery methods carrying a GFP payload to RAW264.7-IRCs at timepoints of 24 hours and 48 hours post-delivery. %GFP+ representing efficient delivery and %mCherry+ representing inflammatory response. Percentages represent the average of 3 biological replicates. Each bar represents the average percentages from 3 biological replicates. TransIT-X2 and Lipofectamine 2000 were only evaluated at 48 hours post-transfection per manufacturer protocol. Raw data points can be found in Table S4.

2B. Evaluation of the geometric mean of GFP to mCherry at 24 and 48 hours post-delivery. The data represented here is the same samples in 2A. Individual data points were plotted for each biological replicate. Y-axes between 24 and 48 hours is different. Raw data points can be found in Table S4. Statistics done using One-Way Anova and Tukey's Post-Hoc Analysis can be found in Table S5 for 24-hour and S6 for 48-hour.

2C. Representative cell populations from dual-fluorescence reporter assay. Populations represented here are RAW264.7 cells with no reporter to set the negative control for GFP/mCherry, non-treated RAW264.7-IRCS (NT) to determine basal mCherry expression among reporter cells, and then three representative populations from RAW264.7-IRCs treated with AAV 1, Ad 5/35, and TransIT-X2, respectively. Gating strategy for dual-fluorescence assay can be found in Figure S2.